The Response to Orbital Perturbations in an Atmospheric Model Coupled to a Slab Ocean

PETER J. PHILLIPPS AND ISAAC M. HELD

Geophysical Fluid Dynamics Laboratory/NOAA, Princeton, New Jersey

(Manuscript received 23 March 1993, in final form 24 August 1993)

ABSTRACT

The sensitivity of an atmospheric GCM coupled to a mixed-layer ocean to changes in orbital parameters is investigated. Three experiments are compared. One has perihelion at summer solstice and a large obliquity; another has perihelion at winter solstice and a low obliquity. The first of these is favorable for warm summers; the second for cool summers. A third experiment, with perihelion at summer solstice and the lower value of obliquity, is used to examine the relative importance of the changes in perihelion and obliquity. The eccentricity is set at 0.04 in all cases.

Surface temperature responses are as large as 15°C, with the largest response over North America in summer. Changes in monsoons and Arctic sea ice are consistent with previous GCM studies. A perpetual summer version of the atmospheric model is used to investigate the positive feedback due to soil moisture. Drying of the soil over North America is found to increase the temperature response by approximately 50% and is also essential to the decrease in summertime precipitation in that region. Soil moisture changes also enhance the precipitation response over central Africa, but have little effect on the model's Asian monsoon.

The orbital parameters most favorable for expansion of the Northern Hemisphere glaciers, that is, minimal seasonality, do not produce permanent snow cover. Several model deficiencies that act to accelerate the melting of snow in spring may be responsible.

1. Introduction

While paleoclimatic records provide considerable evidence in support of the astronomical, or Milankovitch, theory of the ice ages (Hays et al. 1976), the mechanisms by which the orbital changes influence the climate are still poorly understood. Models that focus on the atmosphere can only provide part of the answer to the puzzle of the glacial fluctuations, perhaps a rather small part. The slow response of the glaciers to their changing environment and their feedback onto the climate complicates the problem by creating large time lags; even on the long time scales over which the orbital parameters vary, one cannot think of the climatic state as being one of equilibrium. There are also compelling reasons to believe that both the deep ocean circulation and the changing atmospheric CO_2 concentration play important roles in determining the climatic response. Despite these complications, there is a need to understand the atmospheric response to orbital perturbations more fully, both to better understand what can and cannot be explained from the atmospheric response alone, and to analyze the responses of the relevant forcing functions for the more slowly evolving parts of the system.

Corresponding author address: Dr. Isaac M. Held, Geophysical Fluid Dynamics Laboratory, Princeton University, P.O. Box 308, Princeton, NJ 08542.

Atmospheric general circulation models, either in isolation or coupled to simple mixed-layer ocean models, are one of the tools that have been used to study the climatic response to orbital perturbations. Kutzbach and Gallimore (1988) and Mitchell et al. (1988) set the orbital parameters to those of 9000 BP, a time when seasonality was increased in the Northern Hemisphere. Both studies find that the Northern Hemisphere monsoon circulations intensify, Arctic sea ice is reduced, and northern midlatitude land temperatures have greater seasonal amplitude. Mitchell et al. find that summertime temperatures over North America are as much as 6°C warmer. Gallimore and Kutzbach (1989) find that the inclusion of soil moisture feedback increases the summer surface temperature sensitivity. Oglesby and Park (1989) study the effect of the perihelion angle on the climate of the Cretaceous period, and find that the monsoon circulations intensify with increased seasonality of insolation, especially in the Northern Hemisphere, just as in studies of the Pleistocene climate. Park and Oglesby (1990) also study obliquity effects on monsoon circulations, and find these effects to be weak. Rind et al. (1989) use various combinations of orbital parameters, sea surface temperatures, imposed land ice, and CO_2 concentrations in a GCM to investigate glacier initiation. They find that land surface snow cover is not maintained through the summer over North America or Scandinavia even when all these model parameters are set at values thought to be favorable for glacial growth.

For this study, we utilize the atmosphere–mixed layer ocean model developed by Manabe and collaborators at the Geophysical Fluid Dynamics Laboratory. Essentially the same model has been used to study the climatic response to an increase in atmospheric CO_2 (Manabe and Stouffer 1980) and to investigate the contribution of various factors to the climate of the last glacial maximum (Broccoli and Manabe 1985, 1987). In examining this model's sensitivity to different orbital parameter combinations, we have compared three numerical experiments.

Our starting point was to choose the two experiments that are likely to generate the largest differences in climate, given the range of the parameter variations computed to have occurred over the past few hundred thousand years. The eccentricity is set equal to 0.04 in both cases. This is considerably larger than the present value of 0.016 but comparable to that which existed from ~90 to 150k BP. In the first experiment, the perihelion is located at Northern Hemisphere summer solstice and the obliquity is set at the high value of 24°. In the second case, perihelion is at Northern Hemisphere winter solstice and the obliquity equals 22°. The perihelion and obliquity are both favorable for warm northern summers in the first case, and for cool northern summers in the second, while the large value of the eccentricity accentuates the effect of the perihelion shift. These experiments are referred to as WS and CS, for "warm summer" and "cold summer," respectively.

We then performed another calculation to determine how much of the difference between these two integrations is due to the perihelion shift, and how much to the change in obliquity. This third model has perihelion at summer solstice, but a low value (22°) of the obliquity. The eccentricity is still set at 0.04. This experiment is referred to as WS22.

Further details on the model are provided in section 2. The results from the first two seasonal integrations are presented in section 3. The third calculation, and the separation of the response into the parts due to the perihelion and obliquity changes, is described in section 5.

Our focus is primarily on the summertime climate, with an eye toward the extent to which the model with cool summers is consistent with the initiation of a continental ice sheet. To help interpret the patterns of temperature and precipitation that result, we have also examined a series of perpetual July integrations with the atmospheric model in isolation, using different combinations of the forcing and the boundary conditions (sea surface temperature, sea ice distribution, and soil moisture) provided by the seasonal coupled model. These perpetual July integrations are described in section 4.

We find that the favorable orbital configuration is far from being able to maintain snow cover throughout the summer anywhere in North America. This problem is discussed in section 6.

2. The seasonal GCM

The atmospheric component of the model is spectral, with rhomboidal truncation at wavenumber 15, and is finite differenced in the vertical, utilizing sigma = pressure/(surface pressure) as the vertical coordinate, with nine unequally spaced levels. Moist convection is accounted for with the convective adjustment scheme of Manabe et al. (1965). Clouds and ozone concentrations are fixed functions of latitude, and vertical level, while water vapor is fully interactive with the radiative transfer. Diurnal variation of insolation is ignored, and land is assumed to have zero heat capacity. Evaporation from land is a function of the "soil moisture" that is computed by the "bucket method" described by Manabe et al. (1969). The same "bucket method" is widely used in many other climate models, including those used for the study of summer dryness associated with CO_2 warming. We chose to use it here for consistency with previous studies. The albedo of bare soil is taken from Posey and Clapp (1964); the albedo of snow-covered surface is a function of depth and temperature, with a maximum of 60% for snow below −10°C and deeper than 2-cm water equivalent.

Over the oceans, the model simply has a stagnant slab of water 50 m deep that provides the heat capacity needed to obtain roughly the correct magnitude for the seasonal oceanic heat storage. Sea ice is predicted by a simple thermodynamic model. Its albedo is a function of thickness and temperature. Albedo for ice over 1 m thick ranges from 55% at 0°C to 80% at −10°C. The ice sheets on Antarctica and Greenland are given their present-day heights, and surface albedos ranging from 55% to 80% depending on temperature, presence of snow and snow depth.

The model ignores two important mechanisms, cloudiness variations and oceanic heat transport, either of which can grossly alter climatic sensitivity. The choice to fix cloud amounts and optical properties is based partly on our lack of confidence in cloud prediction schemes and partly on the fact that, in any case, one needs the climatic response with fixed clouds to study and evaluate the effects of the cloud feedback. The omission of oceanic heat transport causes substantial bias in the model (the North Atlantic is too cold, the equatorial Pacific temperatures too zonally symmetric, etc.). In a similar model, Hansen et al. (1988) specify a nonzero oceanic heat flux at the base of the model's "mixed layer" so as to force the model's sea surface temperatures close to those observed in the present climate. They then assume that this flux is unchanged as they perturb the model. This does not appear to cause severe problems when the climate warms, but when the climate cools we suspect that the advance of the sea ice can be controlled by the imposed oceanic heat flux in an implausible manner. We choose not to employ this strategy here and simply set the oceanic heat flux equal to zero, accepting the distortions of the

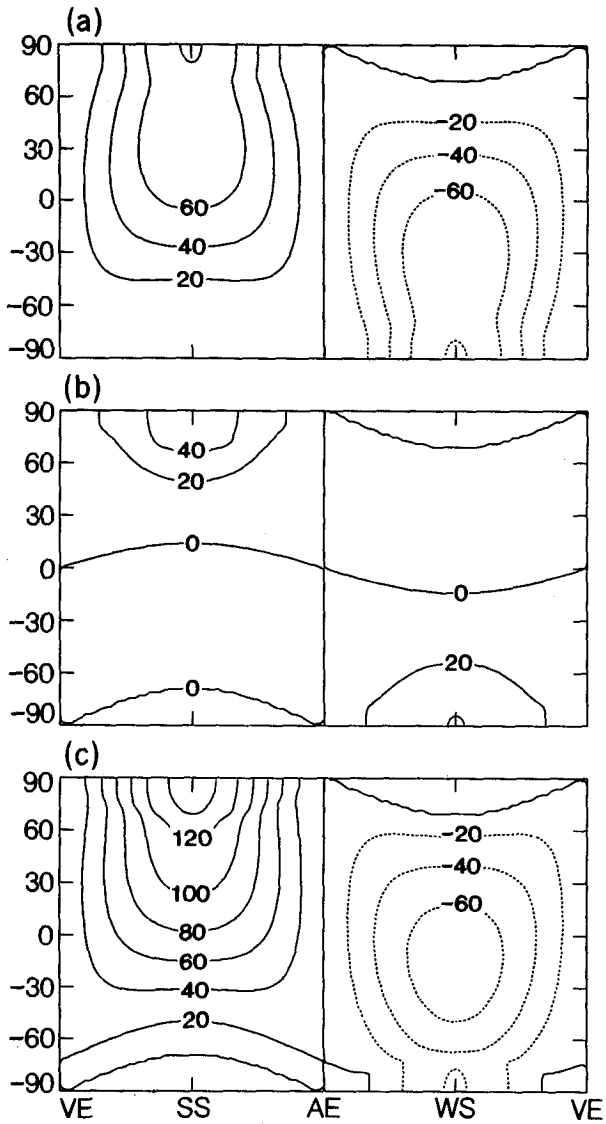

FIG. 1. Differences in insolation at top of atmosphere (W m^{-2}). (a) WS22 minus CS (effect of shift in perihelion from summer to winter solstice; (b) WS minus WS22 (effect of obliquity increase from 22° to 24°); (c) WS minus CS (sum of perihelion and obliquity effects). Note that the ordinate is celestial longitude rather than time.

climate that result, such as excessive sea ice in the North Atlantic and in the Southern Ocean.

The diurnally averaged solar irradiance at the top of the atmosphere is computed from the orbital geometry. The increase in the irradiance at summer solstice due to the shift in perihelion from winter to summer solstice is $\sim 4\epsilon S$, where S is the irradiance for a circular orbit and ϵ the eccentricity. For $\epsilon = 0.04$ and a planetary albedo of 0.30, this amounts to an increase of ~ 55 W m^{-2} in the absorbed flux at 45° at summer solstice. The obliquity increase from 22° to 24° adds an additional 10 W m^{-2}. While the obliquity effect on the irradiance at summer solstice is much smaller than that of the perihelion shift (see Fig. 1), it is presumably more important for those parts of the system, such as the oceanic temperatures and the sea ice, that are more sensitive to the annual mean irradiance. The obliquity increase causes an increase of 8 W m^{-2} in the annual mean absorbed flux at the poles (assuming a planetary albedo of 0.4). The perihelion shift has no effect on the annual mean irradiance. The reader is referred to Suarez and Held (1979) for further discussion of the latitudinal and seasonal structure of the insolation anomalies associated with these orbital perturbations.

The atmosphere–mixed-layer model is integrated with the WS orbital forcing (perihelion at summer solstice, obliquity = 24°) for 30 years. The final state from this run is then used to initialize the other two calculations, which are each integrated for an additional 35 years. The last 10 years of each integration are used to define the model's climate. Inspection of the slowly evolving parts of the system, the sea ice distribution in particular, shows no obvious trends during this analysis period.

The perpetual July atmosphere-only model is integrated for 800 days, the final 600 days being used for analysis of the climatic responses.

3. Response to extremes in summer insolation

The difference in annual mean surface temperature as a function of latitude between the "warm northern summer" (WS) and "cold northern summer" (CS) cases is displayed in Fig. 2. Warm northern summer is warmer by nearly 4°C at high northern latitudes in the annual mean, cooler throughout the tropics and warmer at high southern latitudes. The pattern of this annual mean temperature response is similar to that of the annual mean insolation anomaly due to the ob-

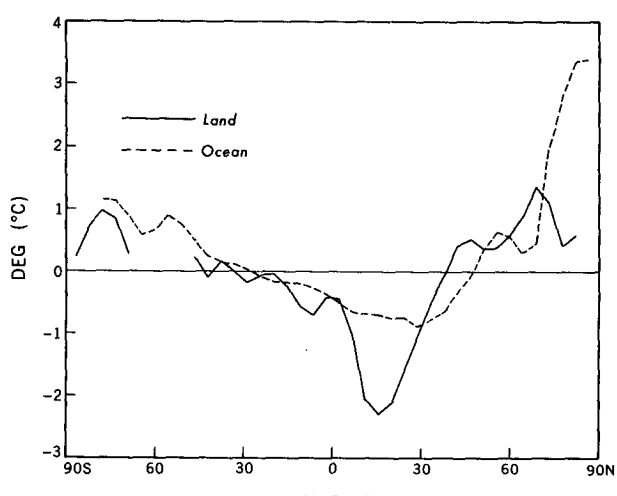

FIG. 2. Difference in zonal annual mean surface temperature (degrees Celsius) between the WS and CS experiments for land and ocean.

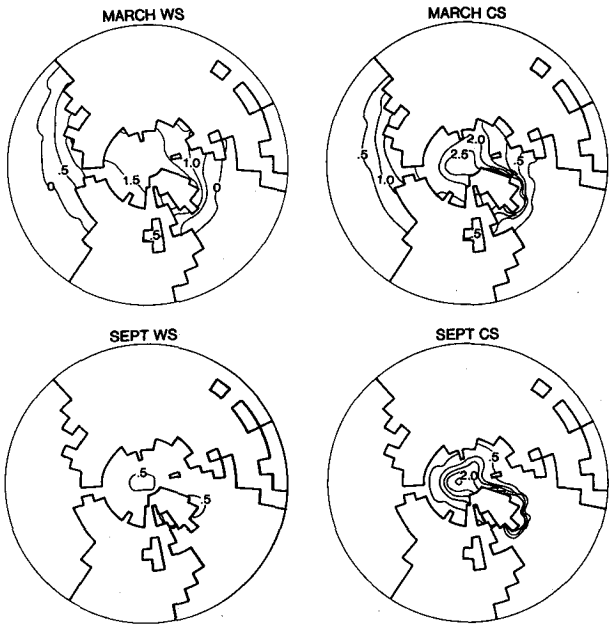

FIG. 3. Arctic sea ice thickness (meters) for the CS and WS experiments for March and September.

liquity change, which redistributes insolation from low to high latitudes, a point that we return to in section 5.

The annual mean cooling of the land surface near 20°N is associated with intensification of the summer monsoon circulations over Africa and Southeast Asia. In these regions, the increased summer precipitation results in wetter soil and greater evaporation from the surface. This tends to negate the effect of increased insolation on surface temperatures. In winter the surface temperature responds more strongly to the negative insolation anomaly, so that the change in the annual mean follows the change in winter. Note that most land at 20°N is in regions of monsoonal climates in Africa and Southeast Asia.

The warming at high northern latitudes is associated with a dramatic reduction in sea ice. The March and September sea ice thicknesses are shown in Fig. 3. Figure 4 shows the annual cycle of sea ice thicknesses at one arctic grid point near the pole, where it is generally thickest throughout the year for all orbital configurations. For WS, the arctic ice barely survives the summer as a small thin (<0.5 m) patch near the pole, and at few points near the Greenland coast; in CS, ice still covers most of the Arctic at the time of minimum extent (September), and the minimum thickness is over 2 m at the pole. The maximum sea ice extent is greater than observed, even in the WS climate, partly because of the absence of oceanic heat transport in the model.

The annual mean temperature response is an average over much larger changes in seasonal temperatures. Figure 5a shows the surface temperature difference (WS

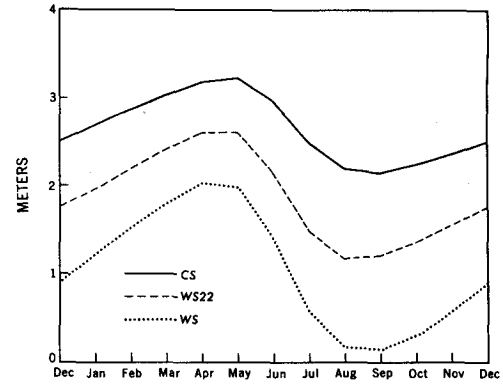

FIG. 4. Annual cycle of sea ice thickness (meters) at a model grid point near the North Pole, where the ice is generally the thickest.

− CS) in July. The warming is very large over the northern continental interiors, reaching 9°–12°C in central Asia and >15°C in central North America. The amplitude of the temperature change in the atmosphere near the ground is slightly smaller, reaching 12°C in the latter region, but the spatial pattern closely follows that of the surface temperature change.

The temperature changes in January (Fig. 5b) are generally of opposite sign, with WS cooler nearly ev-

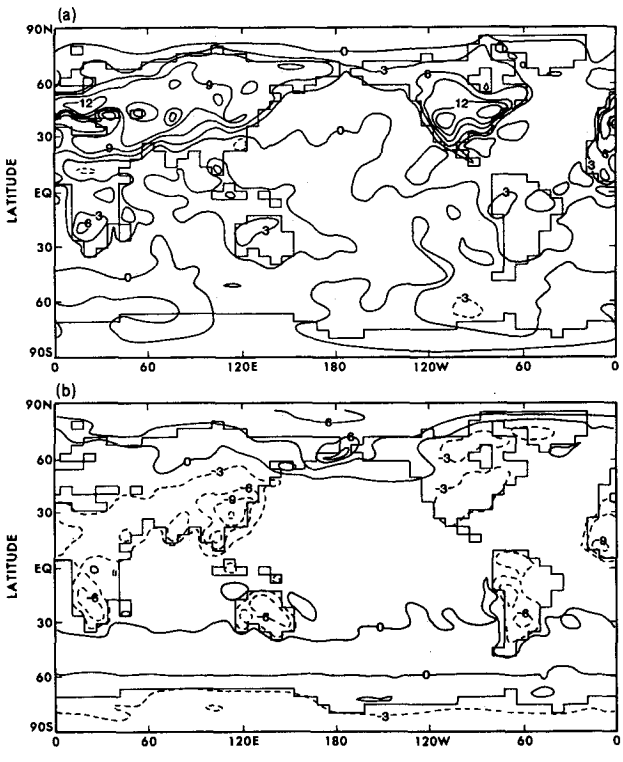

FIG. 5. Surface temperature difference (degrees Celsius) between the WS and CS experiments for (a) July and (b) January. Negative contours are dashed.

erywhere over land. The largest cooling, reaching 12°C, is now over Southeast Asia. The WS model is warmer over the Arctic, due to the thinner sea ice.

The large summertime warming over much of North America and Asia seen in Fig. 5a is intriguing. Part of this warming is a result of the drying of the soil. Figure 6 shows the WS and CS soil moisture distributions and the difference (WS − CS). The drying is particularly well defined along the northern margins of the dry zones in CS. The warming is greatest where the soil has dried in North America, but is also large where the soil was already dry in CS, as in Central Asia. The correlation between soil moisture and surface temperature is investigated further in Fig. 7. In this figure, we have plotted the mean July surface temperature against the mean July soil moisture for each July of both the WS and CS integrations. This is shown for two different model grid points in North America. Also shown are two regression lines for each grid point, one for WS and one for CS. The vertical spacing between the regression lines is a measure of surface temperature sensitivity to insolation. Dry soil temperature is more sensitive to a change in insolation because evaporation contributes little to the surface heat loss and a larger temperature change is needed in order for sensible and longwave heat loss to compensate. This can be clearly seen at grid point A. At point B the soil has dried out almost completely in WS, resulting in the maximum possible sensitivity to insolation. One can question the ground hydrology scheme that produces such dry soil. As discussed by Milly (1991), however, one can modify the model's hydrology so as to reduce the potential

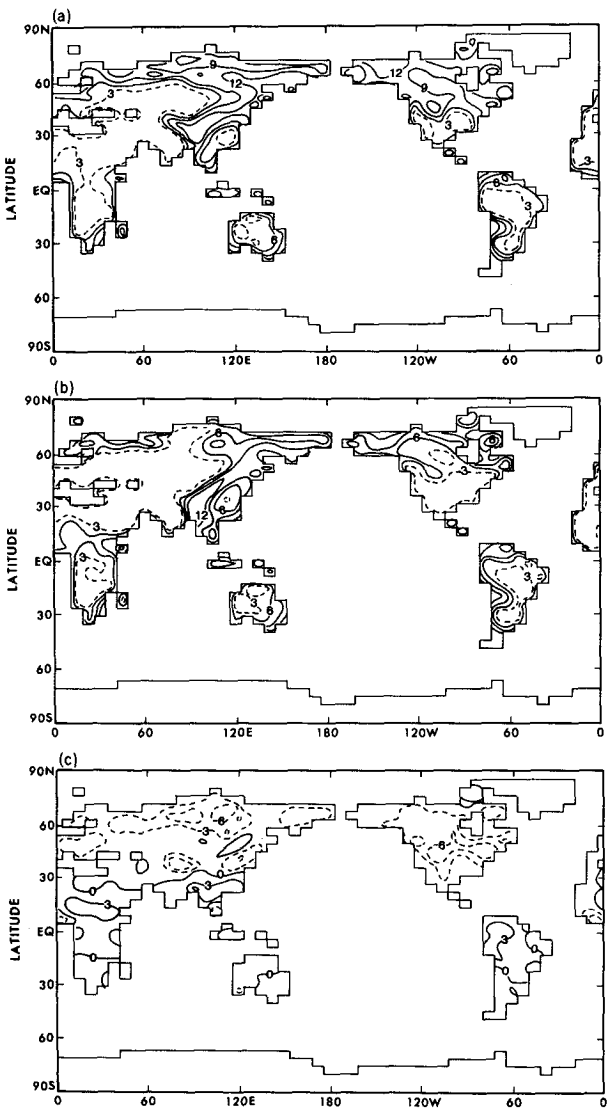

FIG. 6. July soil moisture (cm) from (a) the CS experiment, (b) the WS experiment, and (c) the difference, WS − CS. Negative contours are dashed.

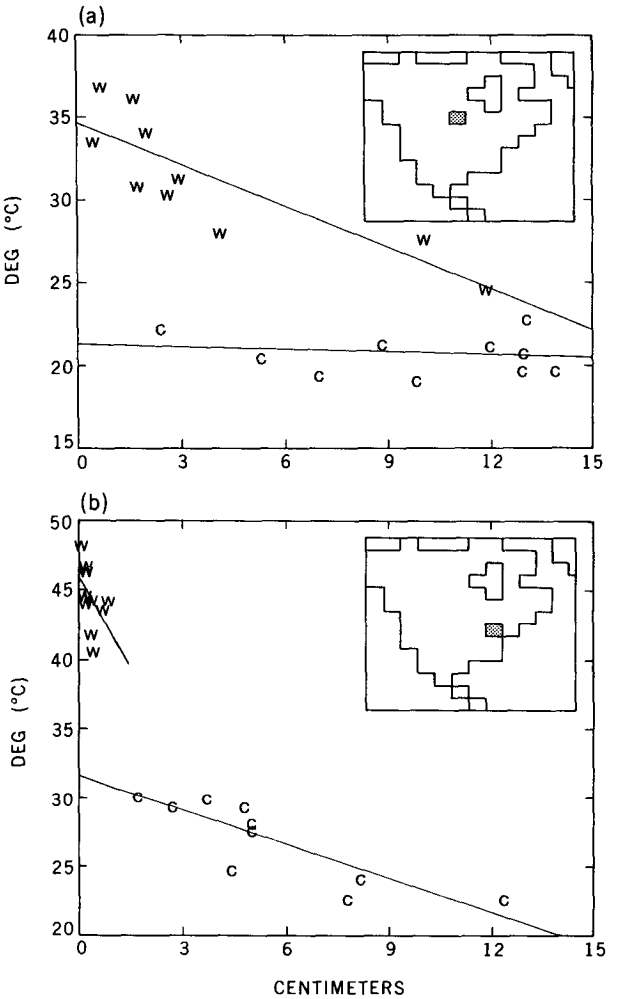

FIG. 7. Surface temperature (degrees Celsius) versus soil moisture (cm) for July. Each point plotted with the letter w represents the month of July for 1 of the 10 years of the WS integration. The letter c represents the same for the CS integration. Each plot is for a single model grid point, the location of which is shown by the insert.

evaporation, but this leads to wetter soil, and the opposing effects of decreased potential evaporation and wetter soil on actual evaporation and on the surface heat budget tend to compensate. Also, the present model has prescribed clouds, and cloud feedback would likely accentuate the soil moisture response, with fewer clouds in the warmer, drier climate.

Figure 8 shows the difference in July precipitation rates between the two experiments. Precipitation increases over north-central Africa, Southeast Asia, and northern South America. Rainfall decreases over much of North America. Because this is the area of largest temperature response, and the large temperature signal is presumably related to the reduction in soil moisture, we examine this reduction more fully in Fig. 9. Plotted are the differences over North America in the surface temperature, soil moisture, evaporation, and precipitation for the individual months from April to August. The dry anomaly and the closely associated temperature signal expand poleward as the warm season progresses. The evaporation increases due to increased insolation over those regions where the soil moisture has not yet been substantially reduced.

The precipitation anomaly in Fig. 9 roughly follows the evaporation, but with a systematic shift poleward. The mean low-level flow (not shown) is southerly east of the Rockies, consistent with this poleward shift. This shift is important, both in generating the pattern of $E-P$ that results in the soil moisture anomalies, and, possibly, in moving these anomalies poleward. The poleward evolution is also likely related to the fact that the region in the model of climatologically very dry soil expands northward with time in the summer, so that the area where there is a potential for soil moisture anomalies, at the northern edge of this region, also shifts northward.

The precipitation anomaly over northern Mexico in April is intriguing, in that it precedes the first signs of a negative soil moisture anomaly in May. Because of the feedbacks present, it is not straightforward to separate the effects of springtime precipitation anomalies on the soil moisture distribution from the effects of the summer insolation anomalies. This issue also arises when studying greenhouse warming. In our case, the change in springtime precipitation appears to be too small to be of central importance.

This study can be compared to that of Mitchell et al. (1988), where orbital parameters are set to 9000 years before present and the climate compared to the corresponding simulation with present-day parameters. Although different atmospheric models are used in the two studies, the soil moisture schemes are identical. The insolation difference between 9000 BP and present is about 40% of that between WS and CS. They obtain changes in summertime surface temperature and soil moisture that are also about 40% of those found in this study, so the results are compatible assuming linearity of response.

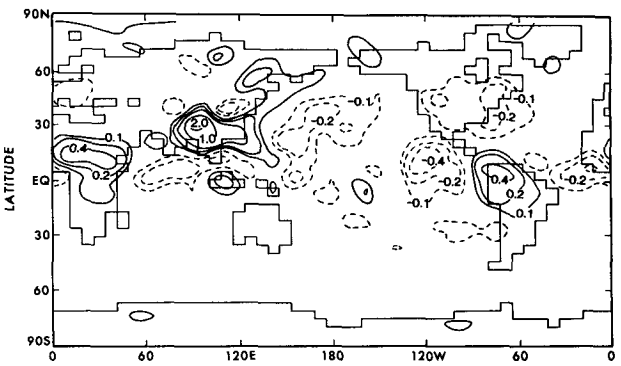

FIG. 8. Precipitation difference (cm day^{-1}) between the WS and CS experiments for July. Contours at ±0.1, 0.2, 0.4, 1.0, 2.0 Negative contours are dashed.

The midlatitude dryness associated with a shift in orbital parameters is reminiscent of that found in many studies of CO_2 warming. Increased potential evaporation in summer is obviously a contributing factor for both types of forcing. A reduction in summer precipitation has also been found in some of the CO_2 studies (Intergovernmental Panel on Climate Change 1990). The major difference lies in the length of the summer drying season. CO_2 warming results in earlier snowmelt and a longer period of soil moisture reduction, but in WS the drying occurs over about the same period of time as in CS.

One must be careful when comparing models with different longitudes of perihelion because of an ambiguity associated with the definition of the time origin. For the preceding analysis, we have set the times (i.e., the calendar day) at vernal equinox equal in the two experiments. Because of the eccentricity of the orbit, autumnal equinox occurs on 10 September for WS and 29 September for CS. If we had chosen a different origin of time, these plots would appear different in detail. See Suarez and Held (1979) for further discussion of this ambiguity.

Despite the large temperature changes on land the CS experiment does not generate any new regions of permanent snow cover over the Northern Hemisphere (as noted in the Introduction, the ice cap over Greenland is prescribed). All snow cover melts away completely in the summer. Thus, the model as presently constituted is unable to initiate the growth of ice sheets from orbital perturbations alone. This is consistent with the results of Rind with a GCM (Rind et al. 1989), but very different from the results of energy balance models such as that of Lin and North (1990) or Hyde and Peltier (1985).

Although reduced seasonality of insolation obviously favors glacial expansion by reducing summer melting, there is another way in which it may contribute. Paleoceanographic evidence indicates that formation of North Atlantic Deep Water was considerably diminished during the last ice age. It has been proposed

TABLE 1. Area-averaged precipitation and evaporation (cm yr^{-1}) over the Greenland and Norwegian Seas. Single asterisk denotes statistical significance for the difference between WS and CS experiments at the 90% level of confidence and double asterisk at the 95% level.

	WS	CS	WS − CS
Precipitation	68.78	72.40	−3.62*
Evaporation	20.85	19.04	+1.81**
P − E	47.93	53.36	−5.42**

(Broecker and Denton 1989) that an increase in precipitation minus evaporation ($P - E$) over the region comprised by the Greenland and Norwegian Seas freshened the surface water, stabilizing the thermohaline structure, reducing North Atlantic Deep Water formation. The resulting change in deep ocean circulation could have cooled the subpolar Atlantic due to reduced penetration of warm surface currents, and might also generate positive feedback by modifying the oceanic carbon cycle so as to lower atmospheric CO_2. If orbital variation alone can substantially alter $P - E$ over the far North Atlantic, without preexisting ice sheets, then it would provide another means by which it could control ice ages. We compare $P - E$ for the CS and WS simulations to determine if the model supports this hypothesis. We use an area that includes all sea points within a rectangle bordered by 62°N and 85°N latitude and 41°W and 34°E longitude. For this area, the annual totals of P, E, and $P - E$ are shown as Table 1 for WS, CS, and the difference (WS − CS). The statistical significance of the differences is tested using a Student's t-test. Indeed, $P - E$ is greater for CS than for WS, and is also statistically significant, but it is not large. Roughly two-thirds of the response is due to the change in precipitation, and one-third to the change in evaporation. Since runoff from land adds freshwater to the ocean, it may be more appropriate to include the land area for this analysis. We find that inclusion of the land area yields about the same magnitude for the response and about the same level of statistical significance. We have also used a larger area to include land and ocean surrounding the Greenland and Norwegian Seas, but this yields a smaller response with lower significance. The relevance of the model to this problem is questionable because the model has no heat flux convergence in its mixed-layer ocean. In reality, the area in question has considerable positive heat flux convergence and remains largely ice free, whereas the model's ocean is ice covered over this area for much of the year.

4. Climate feedbacks in summer

A better understanding of the generation and evolution through the summer of these anomalies requires a more quantitative understanding of the relationship between the precipitation pattern over land and the soil moisture and insolation anomalies. How much of the precipitation anomaly over North America at a particular time of year is forced by the soil moisture distribution? How much would be generated by the change in insolation with fixed boundary conditions? With these questions in mind, we have integrated a perpetual July version of the atmospheric model, using different sets of boundary conditions generated by these coupled atmosphere–mixed-layer ocean experiments.

In this perpetual model, the insolation, ozone, and cloud distributions are all given their July values. (Clouds are once again prescribed.) Ocean temperatures, soil moisture and sea ice distributions are also prescribed, taking these values from the coupled model runs. Four calculations have been performed:

1) insolation from WS, boundary conditions (ocean temperature, soil moisture, and sea ice) from WS;
2) insolation from WS, boundary conditions from CS;
3) insolation from CS, boundary conditions from WS;
4) insolation from CS, boundary conditions from CS.

We refer to these experiments as W/W, W/C, C/W, and C/C, respectively. We must first check that the difference between the perpetual July integrations W/W and C/C is a reasonable approximation to the difference described above in the seasonal model. Figure 10a shows the temperature difference, (W/W) − (C/C). This field is similar in all its major features to that from the seasonal model in Fig. 5a.

The corresponding precipitation difference in Fig. 11a (to be compared with Fig. 8) also accurately mimics the seasonal model's response. The most notable difference is over Central America. Many details in other areas (i.e., east Asia) are captured with fidelity. This agreement also clearly demonstrates the robustness of most of this pattern in both the seasonal and perpetual models.

We can think of the transformation of the CS climate to the WS climate as a process initiated by the change in insolation, then followed by the change in boundary conditions. For this reason, we start by comparing C/C with W/C to isolate the effect of insolation alone, then compare W/C with W/W to determine the additional effect of the altered boundary conditions. These are shown in Figs. 10b,c and 11b,c.

The change in surface temperature over North America due to insolation alone ranges from 3° to 6°C (Fig. 10b). The regions of maximum response do not correspond closely with the regions of maximum response in the full seasonal model or in the W/W − C/C difference.

The additional changes that occur because of the changes in surface boundary conditions (Fig. 10c) are clearly closely associated with the soil moisture anom-

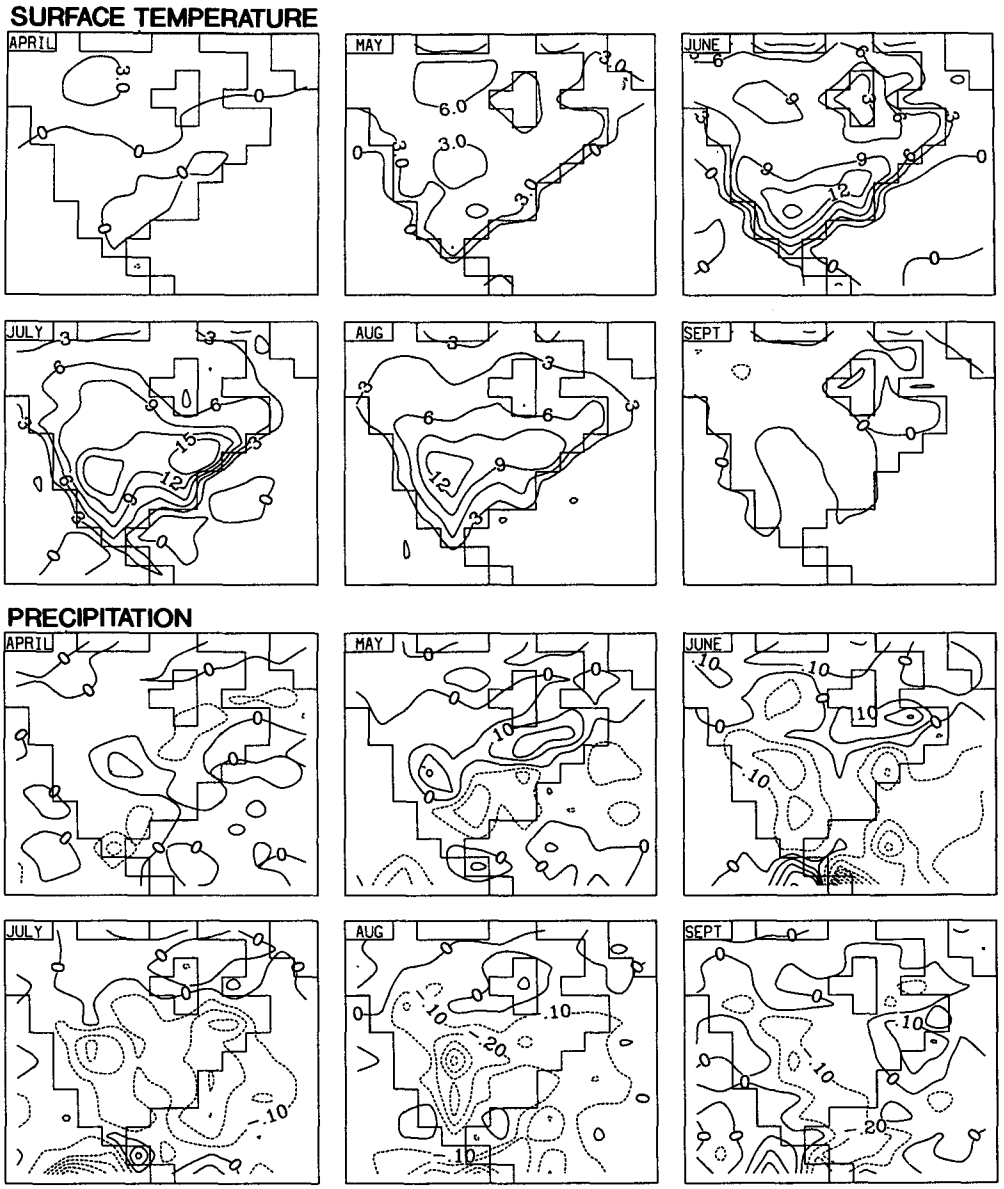

FIG. 9. The progression of differences between the WS and CS experiments through the spring and summer. (a) Surface temperature (degrees Celsius), (b) Precipitation (cm day^{-1}), (c) evaporation (cm day^{-1}), (d) soil moisture (cm). Negative contours are dashed.

alies (Fig. 6c). The changes in sea ice and sea surface temperature could conceivably be playing some role. In the summer, however, the surface temperature of the ice is essentially fixed at the melting temperature, irrespective of the ice thickness, and this temperature is sufficiently close to that of the polar waters that it also matters little if the extent of the ice changes. (It is in the winter that sea ice variations have their greatest effect on the atmosphere.) The changes in ocean temperature are damped by the large heat capacity of the 50-m deep mixed layer, and so are small compared to those over land (Fig. 5a). While further experiments could have been performed to determine whether these oceanic temperature changes are important, the similarity in structure between Fig. 6c and Fig. 10a suggests that the change in soil moisture is the major contributor.

It is a distinct question whether the soil moisture anomalies are themselves a direct response to the insolation anomalies that can be modeled with fixed ocean temperatures, or if ocean temperature changes could also be playing a role in their generation. Again, because the land temperature response to the insolation anomaly is itself substantially larger than the oceanic

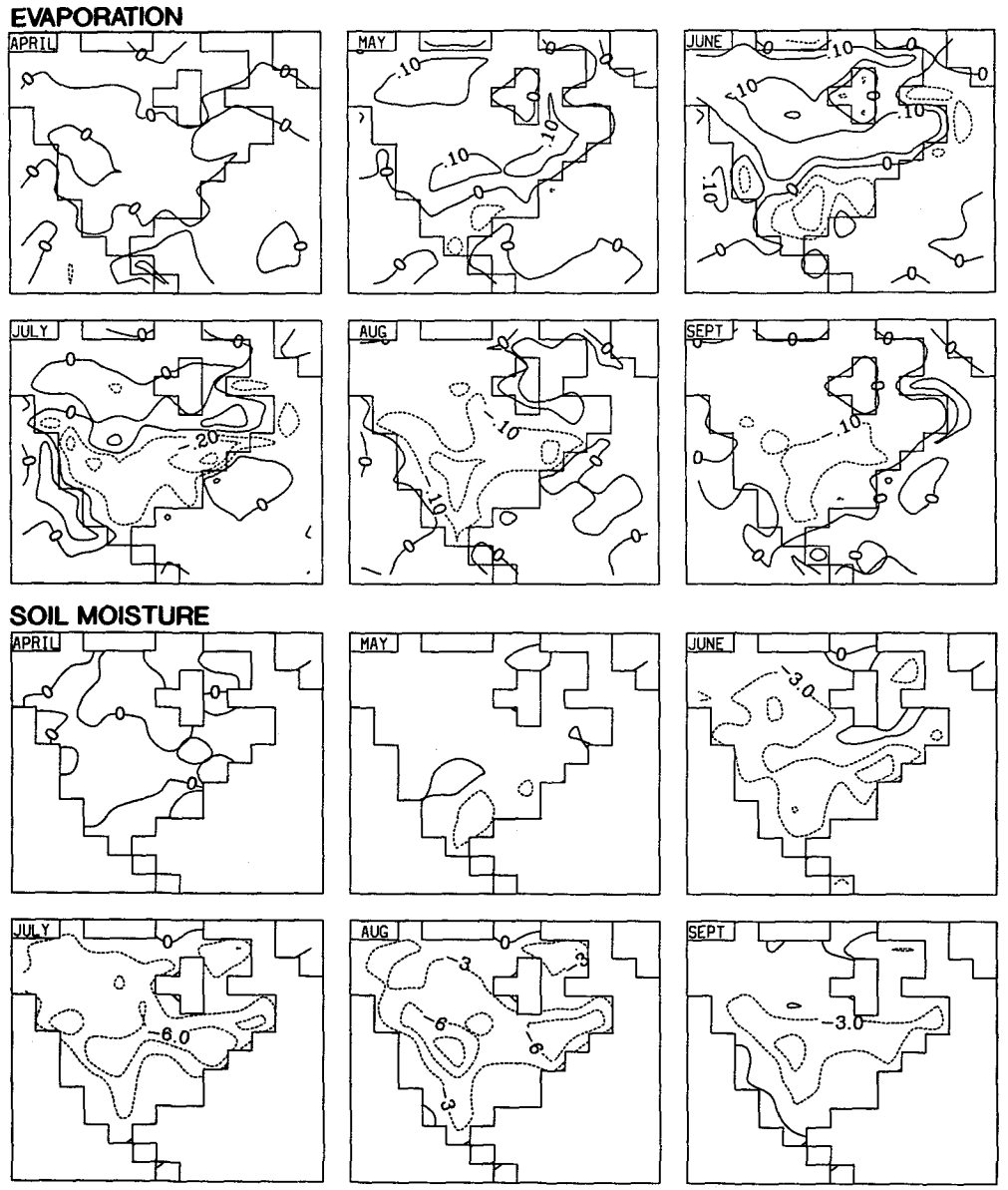

FIG. 9. (*Continued*)

temperature changes, we believe that the soil moisture would respond in a similar way if ocean temperatures were fixed. To confirm this, an additional seasonal integration would have to be performed.

The precipitation response is decomposed in the same way (Fig. 11b and 11c). Much of the signal is evident in the response to insolation alone, particularly over eastern Asia. The contrasts between different regions is striking; the increase in rainfall over east Asia is almost entirely a consequence of the insolation change alone. The increase over central Africa is half due to insolation and half due to the change in boundary conditions. North America is unique in that most of the reduction of rainfall can be simulated only if the boundary conditions (the soil moisture in particular) are modified. There is positive feedback between the insolation induced changes in rainfall and the soil moisture over Africa as well, but the feedback appears to be particularly strong over North America in this model.

The transformation of the WS climate back to the CS climate can again be thought of as a process initiated by insolation, so we compare W/W with C/W then compare C/W with C/C. These are shown for surface temperature as Fig. 12. The insolation change (Fig. 12a) has a slightly greater impact over North America than that seen in Fig. 10b because of the drier soil. Consequently, the effect of boundary conditions (Fig.

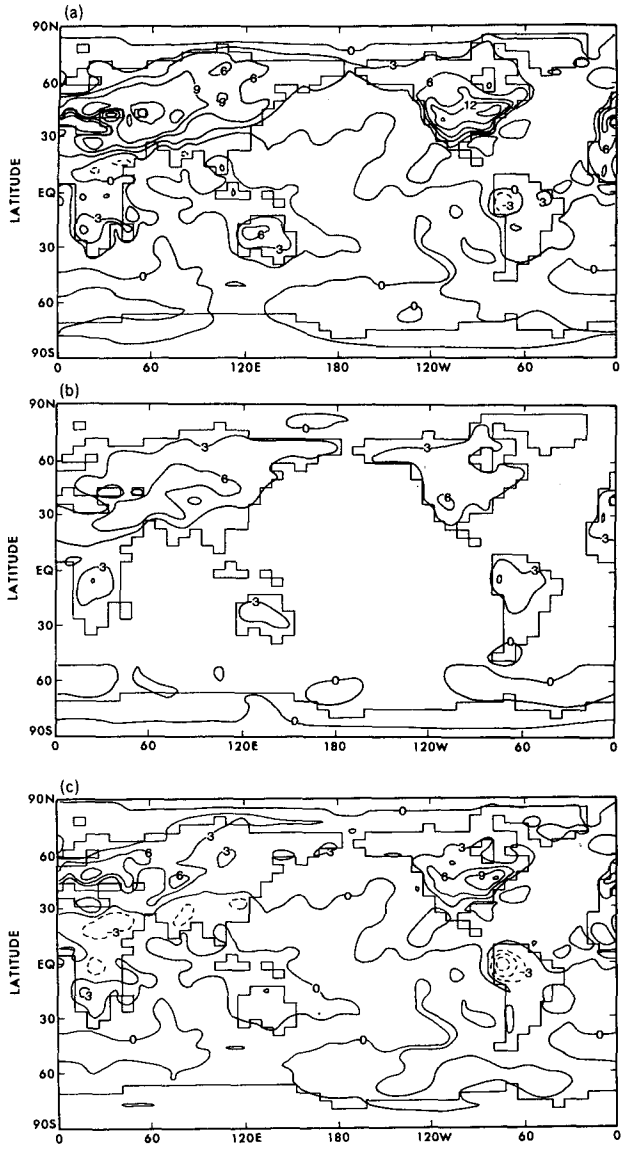

FIG. 10. Surface temperature differences (degrees Celsius) between the following pairs of perpetual July experiments: (a) Insolation and boundary conditions as for WS; insolation and boundary conditions as for CS. (b) Insolation as for WS with boundary conditions as for CS; insolation and boundary conditions as for CS. (c) Insolation and boundary conditions as for WS; insolation as for WS with boundary conditions as for CS.

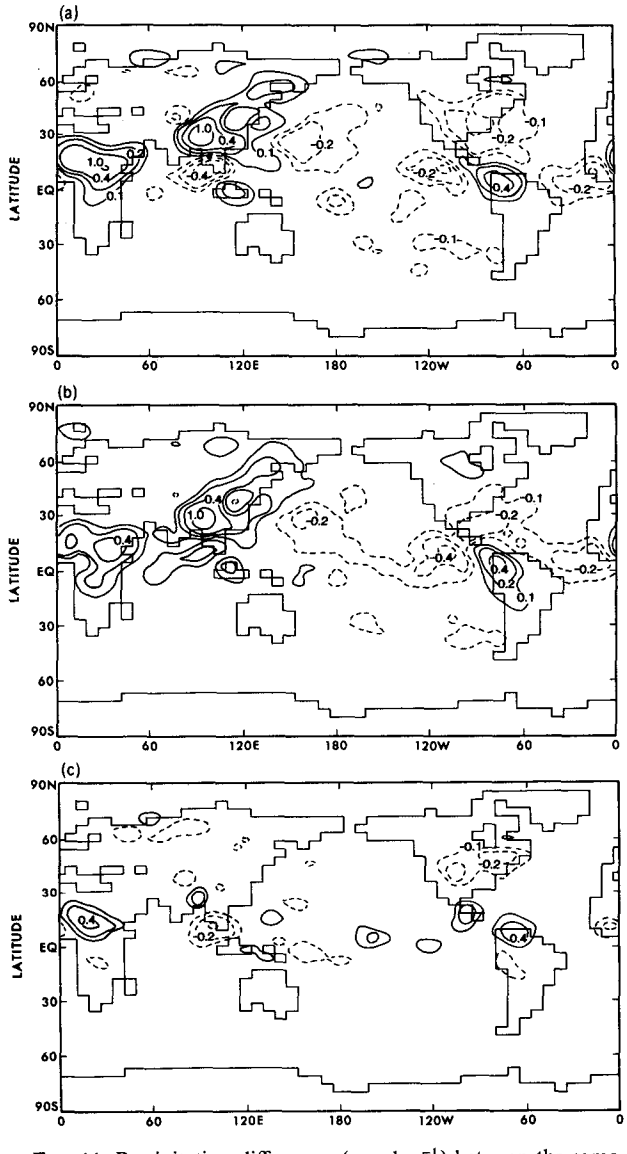

FIG. 11. Precipitation differences (cm day^{-1}) between the same pairs of perpetual July experiments described in Fig. 11. Contours at ±0.1, 0.2, 0.4, 1.0, 2.0. Negative contours are dashed.

12b) is slightly less then that seen in Fig. 10c. Overall, the conclusions drawn previously concerning the role of boundary conditions versus insolation are not altered.

The sensitivity of surface temperature to insolation alone can be compared with that obtained by Kutzbach and Gallimore (1988), where soil moisture is fixed. They compare model climates forced by the orbital parameters of 9000 years before present with those of the present. Assuming that the response of surface temperature is linear with insolation, they obtain sensitivities similar to that seen in Fig. 10b. The same pair of orbital parameters is used by Gallimore and Kutzbach (1989). They compare fixed and interactive soil moisture models. Although their results are qualitatively similar to ours, they obtain less sensitivity in soil moisture and, for fixed soil moisture, greater sensitivity in the surface temperature. The discrepancy between their results and those found in the current study can be explained by differences in the parameterization of evaporation from land. Their parameterization reduces potential evaporation, thereby reducing soil moisture sensitivity. It also increases the Bowen ratio and thereby

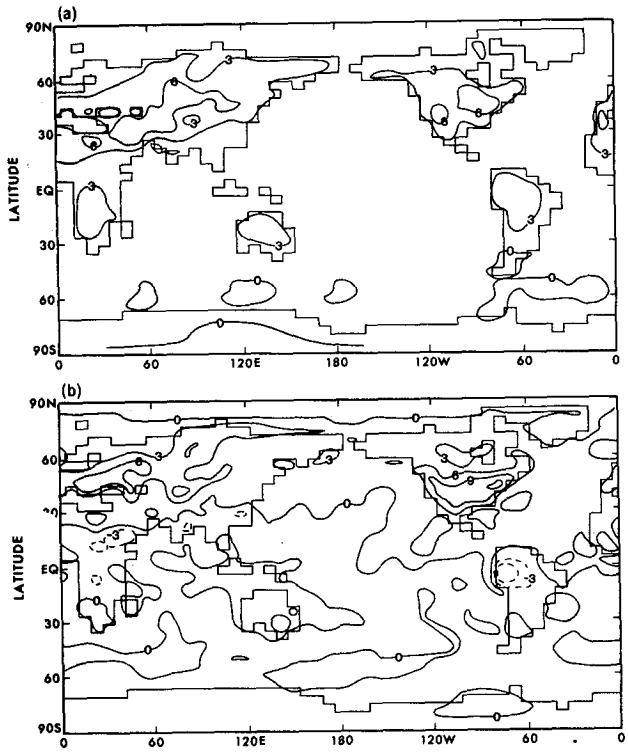

FIG. 12. Surface temperature differences (degrees Celsius) between the following pairs of perpetual July experiments. (a) Insolation and boundary conditions as for WS, insolation as for CS with boundary conditions as for WS. (b) Insolation as for CS with boundary conditions as for WS, insolation and boundary conditions as for CS.

increases surface temperature sensitivity when soil moisture is fixed.

5. Separating effects of perihelion and obliquity

For the simulation referred to as WS22, perihelion is set at summer solstice, as it is for WS, and the obliquity is set equal to 22°, as for CS. Comparisons between WS and WS22 isolate the effect of the obliquity increase from 22° to 24° and comparisons between CS and WS22 isolate the effect of the perihelion shift from winter to summer solstice.

Figure 1 shows that the seasonal redistribution of insolation at the top of the atmosphere due to the obliquity increase is much smaller than that due to the perihelion shift everywhere except near the poles. At a given latitude, however, the annual mean insolation is entirely a function of obliquity alone.

The annual mean surface temperature difference shown as Fig. 2 is decomposed into parts due to obliquity and perihelion and shown as Fig. 13. The effect of the obliquity increase, which is responsible for the redistribution of insolation from the tropics to high latitudes, is to cool the tropics and warm the high latitudes (Fig. 13a). Figure 13b shows the effect of perihelion shift, where no redistribution of annual insolation is involved, but seasonality is increased. The cooling of land near 20°N is associated with increased monsoon circulations, as discussed in section 3. The cooling near 60°N can be explained in terms of seasonal sea ice. The increased seasonality of insolation results in colder winters and thicker seasonal ice. The surface temperature is sensitive to the sea ice thickness in winter, decreasing with increasing ice thickness, and this is reflected in the annual mean.

Figures 14, 15, and 16 show the decomposition of changes in surface temperature, precipitation, and soil moisture, respectively. The surface temperature differences closely follow the changes in insolation. At low to midlatitudes the perihelion shift dominates; the obliquity increase contributes substantially only at higher latitudes. The perihelion shift increases the intensity of the monsoon circulations, which can be clearly seen

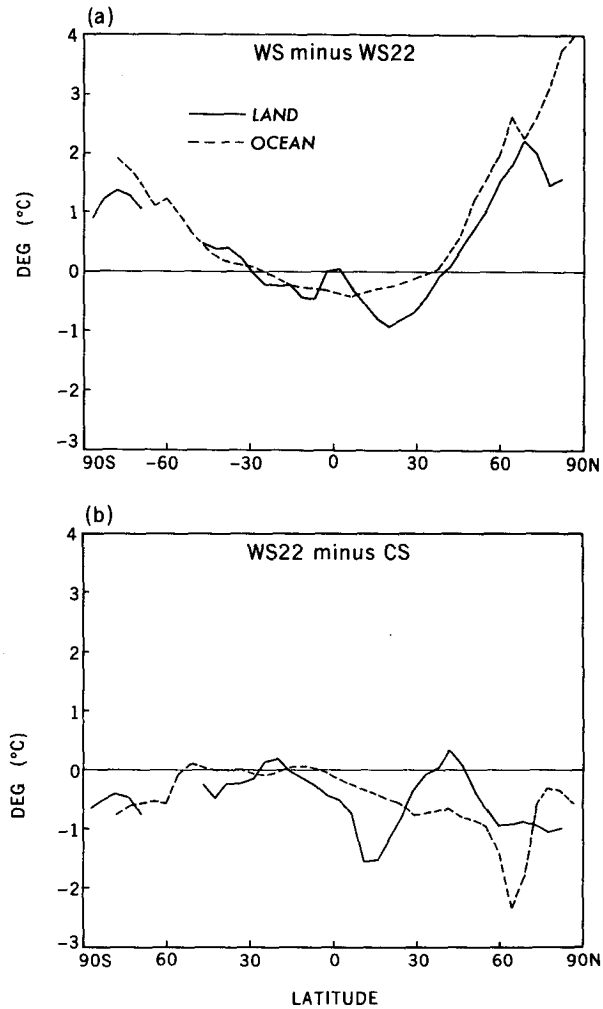

FIG. 13. Differences in zonal annual mean surface temperatures (degrees Celsius) for land and ocean. (a) WS minus WS22; (b) WS22 minus CS.

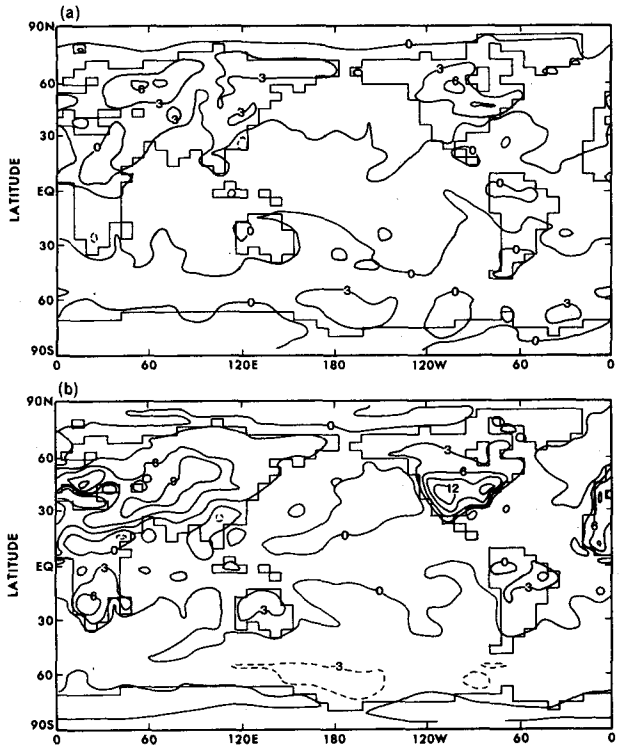

FIG. 14. Differences in July surface temperature (degrees Celsius). (a) WS minus WS22; (b) WS22 minus CS.

in the pattern of the precipitation changes. The obliquity has a surprising and complex effect on the precipitation distribution of the southeast Asian monsoon, however. The drying over North America is predominately due to the perihelion shift.

The September and March sea ice thicknesses for WS22 are shown in Fig. 17. The effect of perihelion shift from winter to summer solstice can be seen by comparing Fig. 17 to CS in Fig. 3. Where the sea ice is permanent, the perihelion shift to summer solstice results in thinner ice year round, despite the fact that the annual mean insolation is unchanged. Because the ice is melting for only a short time near the summer solstice, the amount of melting is strongly dependent on the intensity of insolation at that time. More ice melts when perihelion is at summer solstice and this must be balanced by more freezing in winter. The rate of freezing is proportional to the heat flux through the ice, which is controlled primarily by the ice thickness. The ice becomes thinner in winter so as to allow for greater heat flux and more rapid freezing. (Compare CS and WS22 in Fig. 4.) The seasonal sea ice responds mainly to the winter insolation. Note that the maximum extent of sea ice is nearly identical in WS and WS22, which differ little in winter insolation, but is reduced in CS, where winter insolation is increased (Figs. 3 and 17).

In section 3 we discussed the change in $P - E$ in relation to the formation of North Atlantic Deep Water formation. Using WS22, we can now decompose the $P - E$ change into parts due to perihelion and obliquity. This is shown as Table 2. The change in $P - E$ noted in section 3 can now be seen to be due entirely to the obliquity. The effect of the perihelion shift is not statistically significant.

6. Failure of model to produce permanent snow

Despite cooler summertime temperatures, in CS the winter snow accumulation completely melts during the spring season everywhere except on the imposed glaciers of Greenland and Antarctica. The duration of the snow-free season is at a minimum in the area of Siberia, where it is about 3 months. The July temperature of the arctic land surface is well above freezing; approximately 7°C west of Greenland. The model appears to be far from developing new glaciers.

The model is also unable to maintain a positive ice balance for the Greenland glacier. Table 3 shows the annual ice budget of the Greenland glacier. There are a few points with accumulating snow in the high-altitude interior, as shown by the fact that snowfall exceeds snowmelt. The model treats glacial ice as distinct from snow and the melting of glacial ice plus sublimation more than compensates for the excess of snowfall over snowmelt. As a result, there is net ablation of the glacier

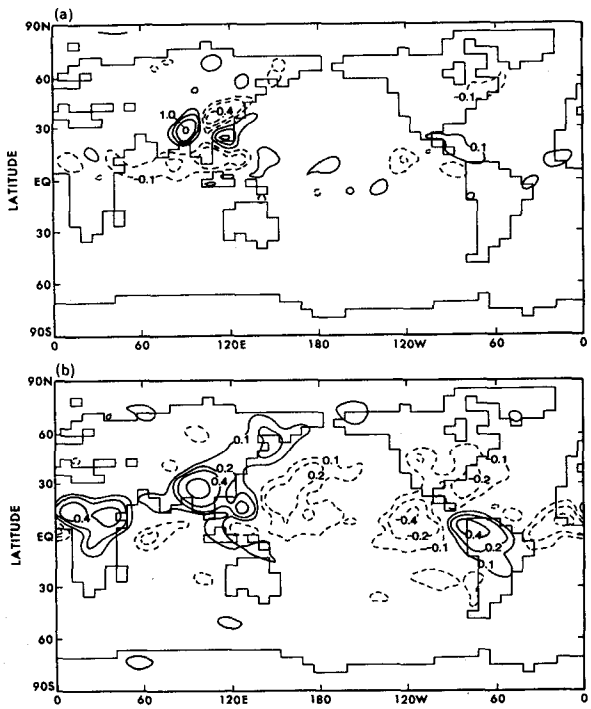

FIG. 15. Differences in July precipitation rates (cm day^{-1}). Contours at ±0.1, 0.2, 0.4, 1.0, 2.0. Negative contours are dashed. (a) WS minus WS22; (b) WS22 minus CS.

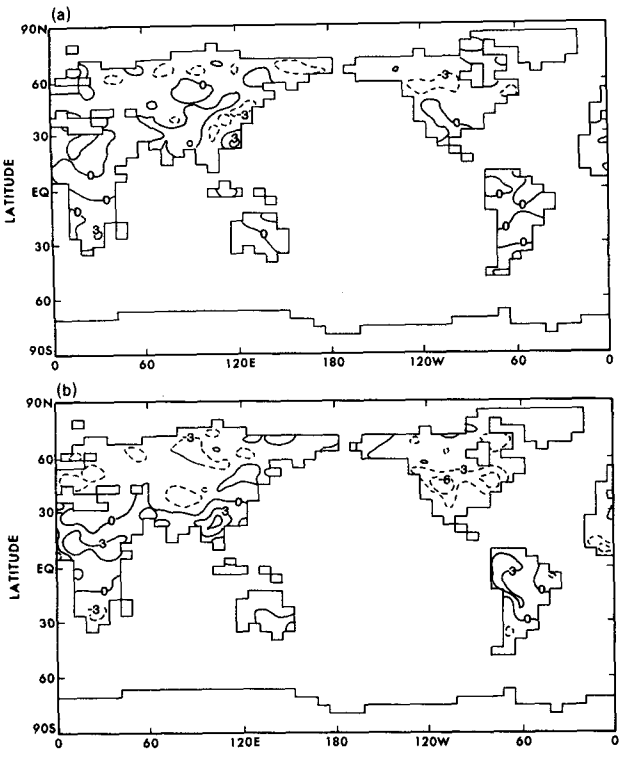

FIG. 16. Differences in July soil moisture (cm). (a) WS minus WS22; (b) WS22 minus CS.

for all three sets of orbital parameters, although CS is rather close to balance. It should be noted here that the model treats all meltwater as runoff; there is no allowance for puddling or for meltwater seeping into the snowpack. This biases the model in favor of ablation of glaciers.

The model's July temperatures have a warm bias in eastern Canada, the region where the Laurentide ice sheet existed; low-level air temperatures for CS are about 2°C warmer than observed and for WS are about 7°C warmer. This bias obviously acts against the inception of a Laurentide ice sheet but, as will be shown by the experiments described below, there are other model deficiencies that appear to be more important in this regard.

To further investigate the model's reluctance to develop permanent snow cover, we perform another experiment by decreasing the solar constant 6% while using the CS orbital parameters. (A 2% reduction in the solar constant is roughly equivalent to a halving of the CO_2 concentration.) The model is integrated to equilibrium, then ten more years for analysis. With this lower solar constant the global mean surface temperature decreases 10.5°C. By comparison, the low-level air temperature is estimated to have been about 4.0°C lower than present at the last glacial maximum (Manabe and Broccoli 1985). The extent of both permanent and seasonal sea ice (not shown) expands far beyond its extent at the last glacial maximum. Despite the large cooling of the model's climate, permanent snow develops only on the Tibetan Plateau. It is conspicuously absent from Canada and Scandinavia. July land surface temperatures in the Arctic are several degrees above freezing, and are less sensitive to the solar constant (5.9°C) than the global mean temperature. The decrease of July surface temperatures from the

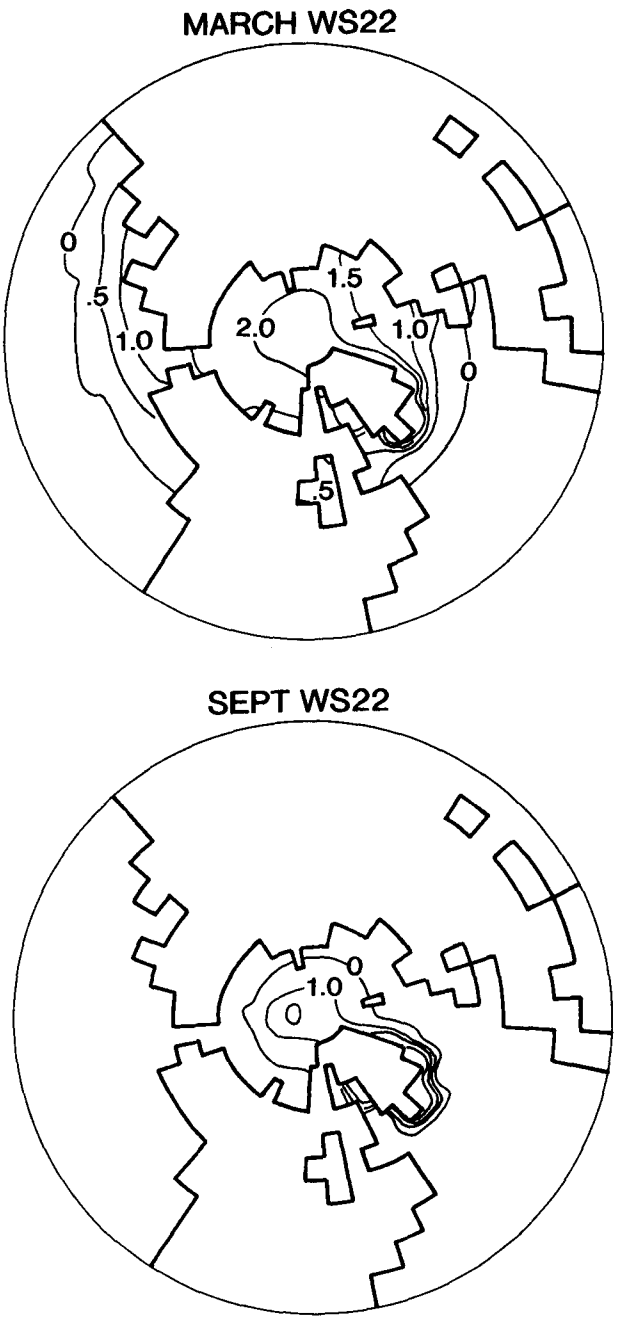

FIG. 17. Arctic sea ice thickness (meters) for March and September for the WS22 experiment.

TABLE 2. Differences in area-averaged precipitation and evaporation (cm yr^{-1}) over the Greenland and Norwegian Seas. Single asterisk denotes statistical significance at the 90% level of confidence and double asterisk at the 95% level.

	WS22 − CS	WS − WS22	WS − CS
Preciptation	+0.18	−3.80*	−3.62*
Evaporation	−1.70**	+3.51**	+1.81**
P − E	+1.88	−7.30**	−5.42**

TABLE 3. Components of the annual ice budget of the Greenland glacier. Units are centimeters per year.

	WS	CS	WS22
Snowfall	+66.4	+71.8	+67.1
Snowmelt	−53.1	−30.1	−49.6
Glacial ice melt	−138.8	−42.0	−87.3
Sublimation	−17.4	−21.0	−19.5
Net	−142.9	−21.2	−89.5

standard solar constant experiment is at most half of what would be needed to bring the arctic land to the freezing point. Such cooling on a global scale without extensive glaciation is not characteristic of past climates.

As a final attempt to produce a realistic ice age initiation, we modify the model's clouds and surface albedos. The low cloud amounts north of 45°N latitude are increased to 70% (from approximately 40% in the standard model), and the albedo of snow is set to 70%, independent of temperature. (The standard model uses 60% as the albedo of snow at a temperature below −10°C, decreasing linearly to 45% at 0°C. Therefore, with the new snow albedo, the fraction of insolation absorbed by melting snow is nearly halved.) These changes have the greatest impact in just those regions where we are looking for permanent snow cover, and a lesser impact globally.

With the solar constant decreased by 3%, permanent snow appears in the area of Alaska as well as the Tibetan Plateau, but is still absent in Canada and Scandinavia (Fig. 18a). As noted above, the unmodified model has a warm bias in the Canadian summer, but in this somewhat arbitrarily modified model, the July low-level air temperatures in eastern Canada are now about 5°C cooler than observed for the present climate.

With the solar constant decreased by 6%, the permanent snow expands into Siberia, western Canada and north-central Canada (Fig. 18b), and the Canadian July air temperatures are about 12°C lower than observed. We now have glaciation, but mainly outside the area where it existed during the last ice age.

We have also explored the possibility that the model's climate possesses multiple equilibria or "small ice cap instability." Would the higher albedo of more extensive snow cover cool the climate enough to maintain it? To test for this possibility, a two-step experiment was performed. Using a solar constant reduced 6% from the standard value, all land north of 45°N was initialized with snow of effectively infinite depth, equivalent to an imposed glacier with no elevation. The model was integrated for 20 years in order to allow the mixed-layer ocean to equilibrate with the imposed snow cover. As a second step, the snow depth was then reduced to a depth of 1-m water equivalent and the model run to equilibrium. The model's climate returned to its original state—no multiple equilibria were found. It is noteworthy that during the last 20 years of integration the snow does not ablate monotonically in all regions. In some regions that are free of permanent snow at the end of the integration, there is a temporary increase in snow depth during the first several years. There is an overall tendency for the snow to ablate from the margins inward, while the interior snow temporarily deepens. Oglesby (1990) performed a similar experiment whereby he initialized a GCM with snow on all Northern Hemisphere land to a depth of 1-m water equivalent. He found that the snow had increased in depth over certain regions after a 400-day integration. He assumed that these were regions where the snow would remain permanent and termed them "glaciation-sensitive." Our result indicates that such an assumption may be unwarranted. Longer integration of his model might have shown these regions to be free of glaciers.

There are several model deficiencies that may be responsible for our model's resistance to the develop-

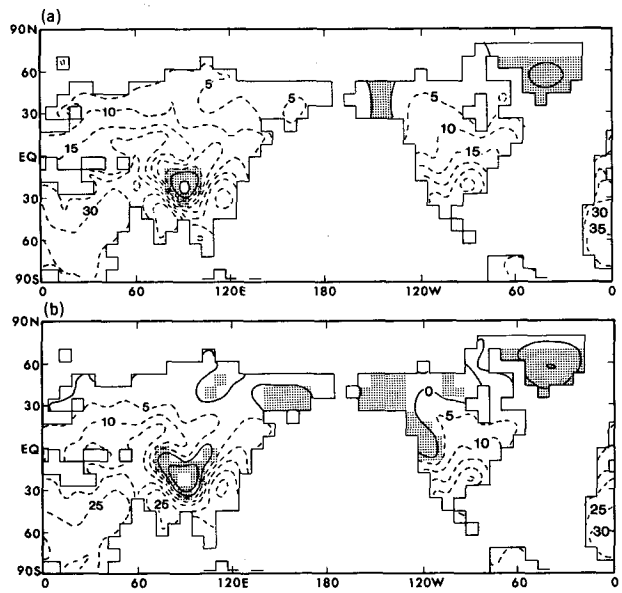

FIG. 18. Annual maximum surface temperature and permanent snow cover for the experiment where low cloud amounts and snow albedo are modified. The maximum monthly mean surface temperature is contoured at 5°C intervals. Model grid points where the minimum monthly mean snow depth is greater than 1-m water equivalent are shaded. (a) Solar constant reduced 3%; (b) solar constant reduced 6%.

ment of permanent snow and that may also bias the ice budget of the model's glaciers in favor of ablation:

1) Course resolution—Smoothing of orography eliminates mountain peaks where cooler temperatures and higher precipitation rates would favor glacier development.
2) Lack of cloud feedback—Fog and low cloud resulting from the advection of warm moist air over incipient glaciers would shield them from insolation.
3) Loss of meltwater—The model does not retain meltwater for possible refreezing. Meltwater either runs off or becomes soil moisture. If the percolation of meltwater into the remaining snow was somehow included, then this water would be available for refreezing.
4) Lack of heat capacity and heat flux in the snow and soil—Snow melts when the surface heat budget yields a net flux into the surface. In the current model, all of this energy is used to melt snow. In reality, some fraction of it would be conducted downward to warm the snow and soil temperatures from their wintertime levels.

7. Summary and conclusions

An atmospheric GCM coupled to a simple mixed-layer ocean model has been used to investigate the sensitivity of climate to changes in the earth's orbital parameters. Three sets of orbital parameters were used, one with high obliquity and perihelion at summer solstice (WS), one with low obliquity and perihelion at winter solstice (CS), and one with low obliquity and perihelion at summer solstice (WS22). In all three, the eccentricity was set to the high value of 0.04. Warm northern summer maximizes seasonality; CS minimizes it. When the WS climate was compared that of CS the following major differences were found:

1) The Northern Hemisphere monsoon circulations intensify in WS, with increased monsoon precipitation, consistent with the models of Kutzbach and Gallimore (1988), Gallimore and Kutzbach (1989), and Mitchell et al. (1988).
2) Land surface temperatures are much hotter in the Northern Hemisphere during summer, as much as 15°C over North America, due to positive feedback involving soil moisture. Winter temperatures are less sensitive.
3) Permanent sea ice is greatly reduced in thickness and extent in the WS climate. The maximum extent of the seasonal ice is not greatly affected.

Since the CS orbital parameters minimize summer insolation and therefore minimize summer melting of snow at high latitudes, CS is the most favorable for the development of permanent snow and expansion of glaciers. The model does not develop permanent snow, however. All snow melts by early summer, albeit a bit later with the CS parameters. This resistance toward the development of permanent snow has been found in other GCMs (Rind et al. 1989). In contrast, energy balance models have been constructed that exhibit much greater sensitivity or abrupt glaciation associated with hysteresis (Suarez and Held 1979; Lin and North 1990).

The WS22 parameters were used to isolate the effects of the perihelion shift and the change in obliquity. Outside of the Arctic region, the shift in perihelion accounts for most of the climate changes. However, the arctic sea ice is strongly affected by obliquity, which accounts for about half of the change in ice thickness.

A perpetual July model was used to separate the effects of insolation and boundary conditions on summer land surface temperatures and precipitation. Insolation alone was found to be primarily responsible for the changes in the intensity of the Northern Hemisphere monsoons, although soil moisture has a substantial effect on the African monsoon, increasing the precipitation response by a factor of 2. Over North America, the changes in soil moisture are responsible for most of the precipitation changes. In the absence of soil moisture anomalies, the temperature increases from CS to WS in central Asia and North America are typically 8°–10°C. The WS22 experiment suggests that approximately ¾ of this change is due to the perihelion shift alone. A temperature change of 6°–8°C is consistent with Gallimore and Kutzbach (1989) and Mitchell et al. (1988), where the temperature response of 3°–4°C is associated with a summer insolation change of about half that between WS and CS. Swings in summertime temperatures of 10°C are to be expected when the eccentricity is as large as 0.04. The paleoclimatic evidence for desiccation of North America and Central Asia at 9000 BP, in contrast to the wetness in Africa, is summarized by Gallimore and Kutzbach (1989). The severity of this desiccation must have been more profound with higher eccentricity and perihelion near summer solstice at 82, 105, and 125 kyr BP.

Given that the model is incapable of initiating a North American ice sheet for the most favorable orbital configuration, one can question whether more exhaustive examination of the model's behavior in response to orbital perturbations is worthwhile. The isolation of the source of this deficiency is a more urgent task.

REFERENCES

Broccoli, A. J., and S. Manabe, 1985: The influence of continental ice sheets on the climate of an ice age. *J. Geophys. Res.*, **90,** C2, 2167–2190.

——, and ——, 1987: The influence of Continental ice, atmospheric CO_2 and land albedo on the climate of the last glacial maximum. *Climate Dyn.*, **1,** 87–99.

Broecker, W. S., and G. H. Denton, 1989: The role of ocean–atmosphere reorganizations in glacial cycles. *Geochim. Cosmochim. Acta,* **53,** 2465–2501.

Gallimore, R. G., and J. E. Kutzbach, 1989: Effects of soil moisture on the sensitivity of a climate model to earth orbital forcing at 9000 years B.P. *Clim. Change,* **14,** 175–205.

Hansen, J., I. Fung, A. Lacis, D. Rind, S. Lebedeff, R. Ruedy, G. Russell, and P. Stone, 1988: Global climate changes as forecast by Goddard Institute for Space Studies three-dimensional model. *J. Geophys. Res.,* **93,** 9341–9364.

Hays, J. D., J. Imbrie, and N. J. Shackeltion, 1976: Variations of the earth's orbit: Pacemaker of the ice ages. *Science,* **194,** 1121–1132.

Hyde, W. T., and W. R. Peltier, 1985: Sensitivity experiments with a model of the ice age climate: the response to Milankovitch forcing. *J. Atmos. Sci.,* **42,** 2170–2188.

Intergovernmental Panel on Climate Change, 1990: Climate change: the IPCC scientific assessment. Cambridge University Press, 366 pp.

Kutzbach, J. E., and R. G. Gallimore, 1988: Sensitivity of a coupled atmosphere/mixed layer ocean model to changes in orbital forcing at 9000 years B.P. *J. Geophys. Res.,* **93,** C1, 803–821.

Lin, R. Q., and G. R. North, 1990: A study of abrupt climate change in a simple nonlinear climate model. *Climate Dyn.,* **4,** 253–261.

Manabe, S., 1969: Climate and ocean circulation. 1, The atmospheric circulation and the hydrology of the earth's surface. *Mon. Wea. Rev.,* **97,** 739–774.

——, and A. J. Broccoli, 1985b: A comparison of climate model sensitivity with data from the last glacial maximum. *J. Atmos. Sci.,* **42,** 2643–2651.

——, J. Smagorinsky, and R. F. Strickler, 1965: Simulated Climatology of a general circulation with a hydrologic cycle. *Mon. Wea. Rev.,* **93,** 769–798.

——, and R. F. Stouffer, 1980: Sensitivity of a global climate model to an increase of CO_2 concentration in the atmosphere. *J. Geophys. Res.,* **85,** 5529–5554.

Milly, P. C. D., 1991: Potential evaporation and soil moisture in general circulation models. *J. Climate,* **5,** 209–226.

Mitchell, J. F. B., N. S. Grahame, and K. J. Needham, 1988: Climate simulations for 9000 years before present: Seasonal variations and effect of laurentide ice sheet. *J. Geophys. Res.,* **93,** C7, 8283–8303.

Oglesby, R. J., 1990: Sensitivity of glaciation to initial snowcover, CO_2, snow albedo, and oceanic roughness in the NCAR CCM. *Climate Dyn.,* **4,** 219–235.

——, and J. Park, 1989: The effect of precessional insolation changes on Cretaceous climate and cyclic sedimentation. *J. Geophys. Res.,* **94,** D12, 14 793–14 816.

Park, J., and R. J. Oglesby, 1990: A comparison of precession and obliquity effects in a Cretaceous paleoclimate simulation. *Geophys. Res. Lett.,* **17,** 1939–1932.

Posey, J. W., and P. F. Clapp, 1964: Global distribution of normal surface albedos. *Geofis. Int.,* **4,** 33–48.

Rind, D., D. Peteet, and G. Kukla, 1989: Can Milankovitch orbital variations initiate the growth of ice sheets in a general circulation model? *J. Geophys. Res.,* **94,** D10, 12 851–12 871.

Suarez, M. J., and Held, I. M., 1979: The sensitivity of an energy balance climate model to variations in the orbital parameters. *J. Geophys. Res.,* **84,** C8, 4825–4836.